# Acoustic emission-based methodology to investigate delamination crack growth under quasi-static and fatigue loading conditions

Milad Saeedifar[1], Mehdi Ahmadi Najafabadi[1], Kaivan Mohammadi[2], Mohamad Fotouhi[3], Hossein Hosseini Toudeshky[4], Reza Mohammadi[1]

## Abstract

The aim of this study was to investigate the applicability of Acoustic Emission (AE) technique to evaluate delamination growth in glass/epoxy composite laminates under quasi-static and fatigue loading. To this aim, Double Cantilever Beam (DCB) specimens were subjected to mode I quasi-static and fatigue loading conditions and the generated AE signals were recorded through the tests. In quasi-static loading, correlations between AE energy with released strain energy and crack growth were established. Then, using the obtained relation the delamination growth curve was predicted by AE method. In next section, delamination propagation under fatigue loading condition was predicted using the established relation between the cumulative AE energy and fatigue crack growth. The predicted crack growth was in a good agreement with the visually recorded data during the tests. The results indicated that the proposed AE-based method has good applicability to evaluate the crack growth during quasi-static and fatigue loading conditions and can be applied in real composite structures to measure the crack length.

**Keywords**

Quasi-Static; fatigue; delamination; acoustic emission; fatigue crack growth

[1] Non-destructive Testing Lab, Department of Mechanical Engineering, Amirkabir University of Technology, Tehran, Iran

[2] Department of Mechanical Engineering, Sharif University of Technology, Tehran, Iran

[3] Advanced Composites Centre for Innovation and Science, University of Bristol, Bristol BS8 1TR, UK

[4] Department of Aerospace Engineering, Amirkabir University of Technology, Tehran, Iran

**Corresponding author:**

 Milad Saeedifar, Department of Mechanical Engineering, Amirkabir University of Technology, Tehran, Iran, Tel: (+98 21) 6454 3466; Fax: +98 21 8871 2838; Email address: milad.saeedifar@aut.ac.ir

# 1. Introduction

Fiber Reinforced Plastic composites (FRP) have many advantages such as high specific strength, specific stiffness, etc. [1-4]. However, these materials suffer from different damage mechanisms, such as matrix cracking, fiber breakage, fiber/matrix debonding and delamination [5-8]. The principal mode of failure in laminated composites is the separation along the interfaces of the layers, viz, delamination [9-14]. This failure results in dramatic reduction of residual strength and stiffness of the structure. Delamination occurs under different loading conditions, i.e. mode I, mode II and mode III. However, mode I delamination is the most common mode of failure occurred in the structures. This is due to lower energy that is required for the initiation of mode I delamination [15-17]

Due to complexity of laminated composites, prediction of fatigue behavior in these materials is not straight forward [18]. Accurate measurement of fatigue crack growth has become a challenging issue in fracture mechanics analyses. Fatigue crack growth monitoring is a difficult and time-consuming test [19]. In addition, work gets harder when the crack is embedded within the structure and could not be seen visually.

Acoustic Emission (AE) is a naturally occurring phenomenon, which is the result of transient elastic wave propagation caused by a sudden release of energy inside the material [20]. There are various sources of AE events in composite materials such as matrix cracking, fiber/matrix debonding, fiber breakage, etc. [21-23]. Recently, AE has been utilized as an applicable technique to detect in-situ information from the damages that occur in laminated composites [5, 24-27].

Some studies have used AE method to investigate the delamination behavior under quasi-static loading condition [28-32]. Fotouhi and Ahmadi [33] investigate initiation of delamination in laminated composites under mixed-mode loading condition using AE method. Arumugam et al. [34] investigated damage mechanisms in glass/epoxy composite specimens under mode I delamination using AE and Fast Fourier Transform (FFT) analysis. Saeedifar et al. [35] determined interlaminar fracture toughness of glass/epoxy composites under mode I, II and mixed-mode I&II loading using AE and Finite Element (FE) methods. The literature review shows that most AE based studies were focused on delamination initiation and there is a lack in the investigation of delamination propagation behavior using AE method.

Due to the complexity of the fatigue phenomenon in composite materials, little work has been done on the behavior of delamination in laminated composites under cyclic loading using AE method. Silversides et al. [36] studied delamination initiation in carbon/epoxy specimens under mixed-mode cyclic loading conditions. Romhany et al. [37] offered an algorithm to predict delamination crack growth in carbon/epoxy specimens subjected to cyclic loading. Romhany's method has two disadvantages: a) to predict the fatigue crack growth at least two AE sensors must be utilized, and b) the accurate AE wave propagation speeds in the specimens must first be calculated.

The aim of this paper is to investigate the delamination propagation in glass/epoxy composites under mode I quasi-static and fatigue loading conditions. The article is composed of two sections. In first section, the delamination behavior under quasi-static loading condition is investigated using mechanical and AE data. Then correlations between AE energy, released strain energy and crack growth are established and quasi-static delamination growth was predicted using AE method. In second section, the

delamination crack growth under fatigue loading is predicted using the AE method. The advantages of the proposed method to predict delamination growth are: predicting delamination growth using only one AE sensor without needing to determine AE wave propagation speed in the specimens. In addition, no AE signals filtering is needed in this method. Consistency of the predicted and visually recorded values for the delamination crack growth, illustrates that AE method is more suitable than the conventional methods for detection of delamination crack growth in the laminated composites under quasi-static and fatigue loading conditions.

# 2 Experimental Procedures

## *2.1 Materials and specimens preparation*

The experimental work was carried out on the epoxy resin reinforced by the E-glass unidirectional and woven fibers with the density of 1.17 $g/cm^3$, 390 $g/m^2$ and 300 $g/m^2$, respectively. The laminates were prepared by hand lay-up. The starter crack was formed by inserting a Teflon film with a thickness of 20 μm at mid-plane during molding as an initial crack for the delamination. The laminated composite test specimens consist of a rectangular shape and uniform thickness consists of 14 plies. Characteristics of the specimens used for this study are illustrated in Fig. 1. For ease of working, the unidirectional specimen $[0]_{16}$ is named U and the woven specimen $[(0-90)]_8$ is named W.
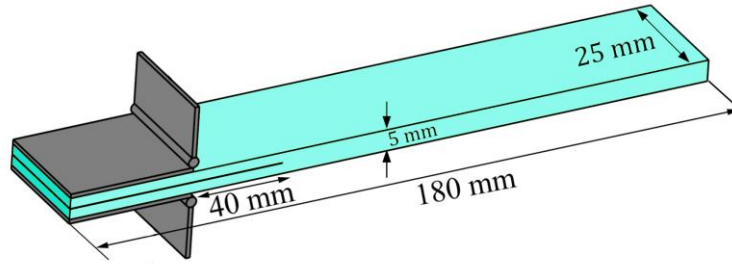
**Fig. 1. The specimens geometry and dimensions.**

## 2.2  Test procedure

### 2.2.1  Quasi-static and cyclic loadings

First, the specimens were examined under quasi-static loading condition according to ASTM D5528 standard [38]. A properly calibrated tensile test machine (HIWA) in the range of 0.5 to 500 mm/min was used in a displacement control mode. The delamination tests were carried out at room temperature and at a constant displacement rate of 3 mm/min. The load and displacement were continuously recorded by the machine and the crack length was recorded using a digital video camera (SONY HDR-XR150) with 25X optical zoom and 300X digital zoom. The fatigue loading tests were performed by a properly calibrated tensile test machine (Dartec) according to ASTM D6115 [39]. Based on ASTM D6115 recommendation the tests were performed under displacement control mod with loading frequency 3 Hz. For ease of working, the quasi-static and fatigue loading specimens are illustrated by 'S' and 'F' subscripts, respectively. The test apparatus is shown in Fig. 2.

**Fig. 2. The experimental setup for quasi-static and fatigue tests.**

### 2.2.2 AE device

AE events were recorded using Acoustic Emission software AEWin and a data acquisition system Physical Acoustics Corporation (PAC) PCI-2 with a maximum sampling rate of 40 MHz. PICO which is a broadband, resonant-type, single-crystal piezoelectric transducer from PAC, was used as the AE sensor. The sensor has a resonance frequency of 513.28 kHz and an optimum operating range of 100–750 kHz. In order to provide good acoustic coupling between the specimen and the sensor, the surface of the sensor was covered with grease. The signal was detected by the sensor and enhanced by a 2/4/6-AST preamplifier. The gain selector of the preamplifier was set to 37 dB. The test sampling rate was 1 MHz with 16 bits of resolution between 10 and 100 dB.

# 3   Results and discussion

## 3.1  Quasi-static loading

### 3.1.1  Mechanical results

Double Cantilever Beam (DCB) specimens were subjected to mode I quasi-static loading according to ASTM D5528 standard [38]. Fig. 3 shows the load- displacement and crack growth-displacement diagrams for specimens $U_{S1}$ and $W_{S1}$. As can be seen, the crack growth in specimen $W_{S1}$ is more stable than specimen $U_{S1}$. This instabilities and rise and fall behaviors in crack growth and load diagrams are called pop-in phenomenon [40]. The big pop-ins in specimen $U_{S1}$ are caused by fiber bridging phenomenon [38, 41-42]. Fiber bridging phenomenon described as the stretching of some fibers between upper and lower layers of the crack plane. This phenomenon occurred at the behind of the crack tip and resulted to the additional resistance against the crack growth [41-42]. When the stress in these fibers reaches to the fibers strength, the fibers are broken and crack abruptly propagates for a few millimeters. By bridging the new fibers, the crack is arrested again. Some small pop-ins in specimen $W_{S1}$ are due to change in the delamination propagation plane that is a common phenomenon in non-unidirectional laminated composites (see Fig. 4).
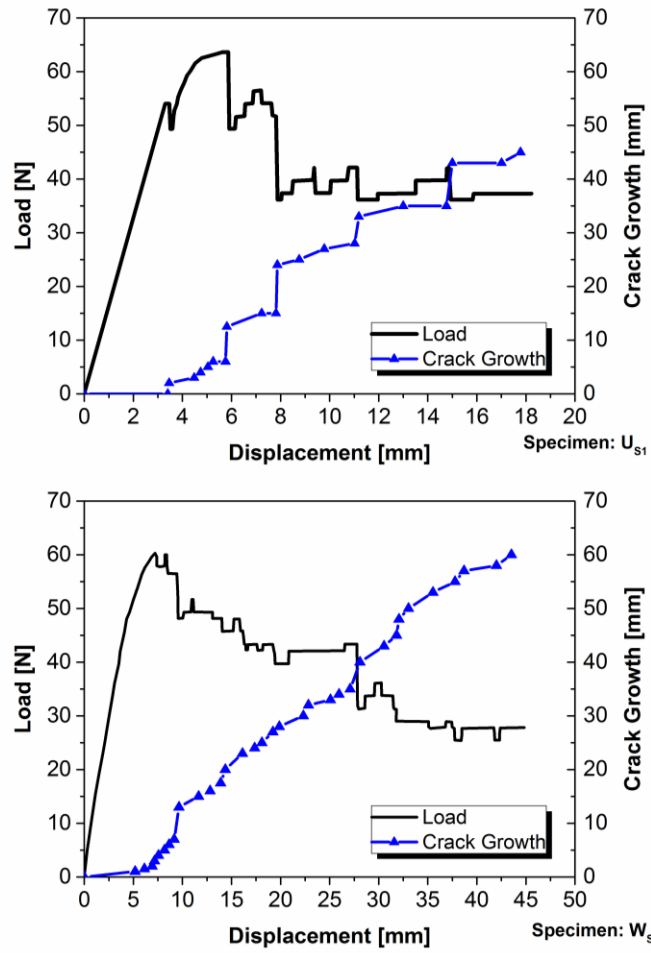
**Fig. 3. Load-displacement and crack growth-displacement diagrams for specimens $U_{S1}$ and $W_{S1}$.**
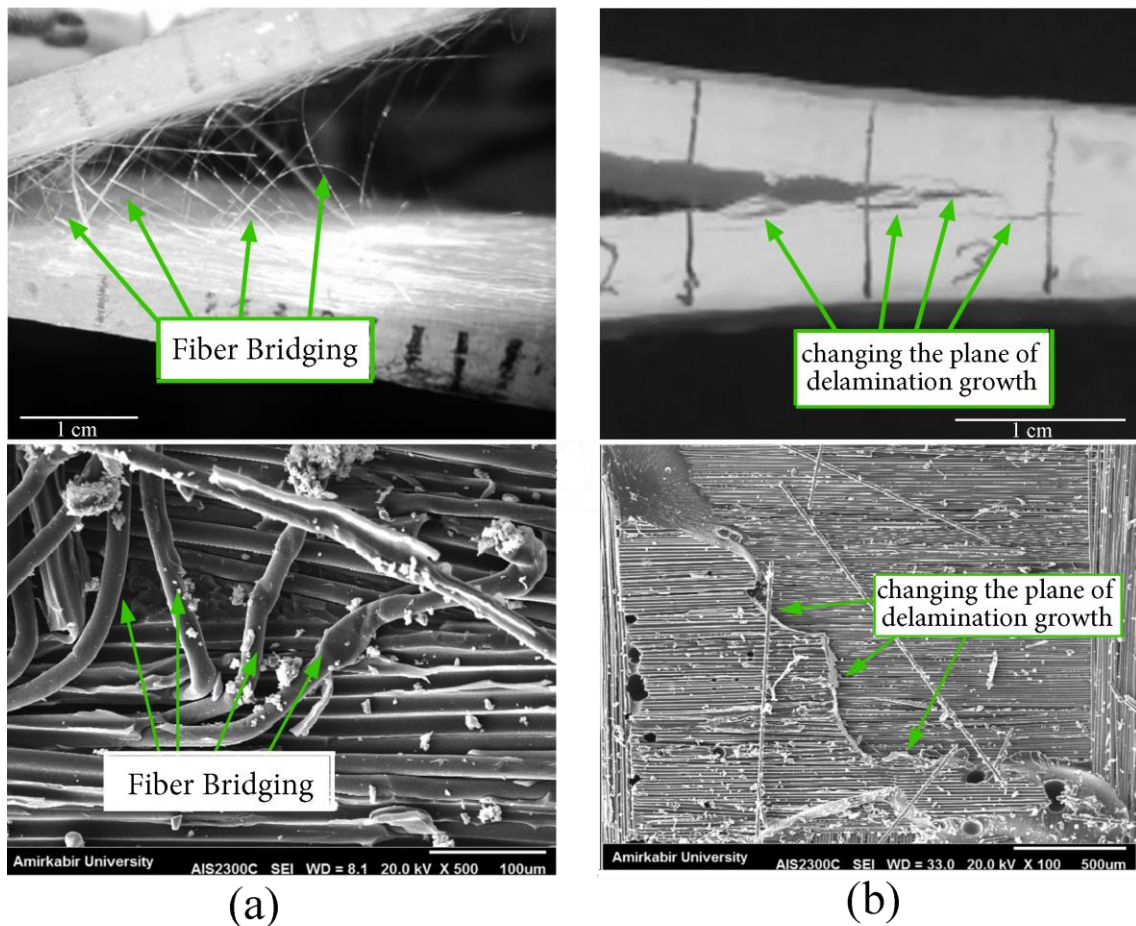
**Fig. 4. Fiber bridging and crack plane changing in specimen a) $U_{S1}$, and b) $W_{S1}$.**

### 3.1.2 AE results

Major damage mechanisms in laminated composites are matrix cracking, fiber breakage, and delamination []. In order to estimate delamination growth using AE method, first, the AE signals of delamination must be specified and discriminated from other damage mechanisms. To this aim, tensile tests of pure resin and fiber bundle were conducted. The pure resin tensile test was performed on a tensile test sample made of epoxy resin and the fiber breakage test was conducted in a tension test on bundle of about 1000 filaments. The AE signals were recorded by the AE sensors that are mounted on the surface of resin and fiber samples (see Fig. 5). According to literature review, best parameters for damage clustering in composite materials using AE method

is peak frequency. It is due to this fact that the peak frequency of a signals does not affected by attenuation. The AE signals of fiber bundle and pure resin tests were analyzed using Fast Furrier Transform (FFT). The frequency range of matrix damage and fiber damage are shown in Fig. 6. As can be seen, frequency range of matrix and fiber damages are [0-150 kHz] and [400-500 kHz], respectively.
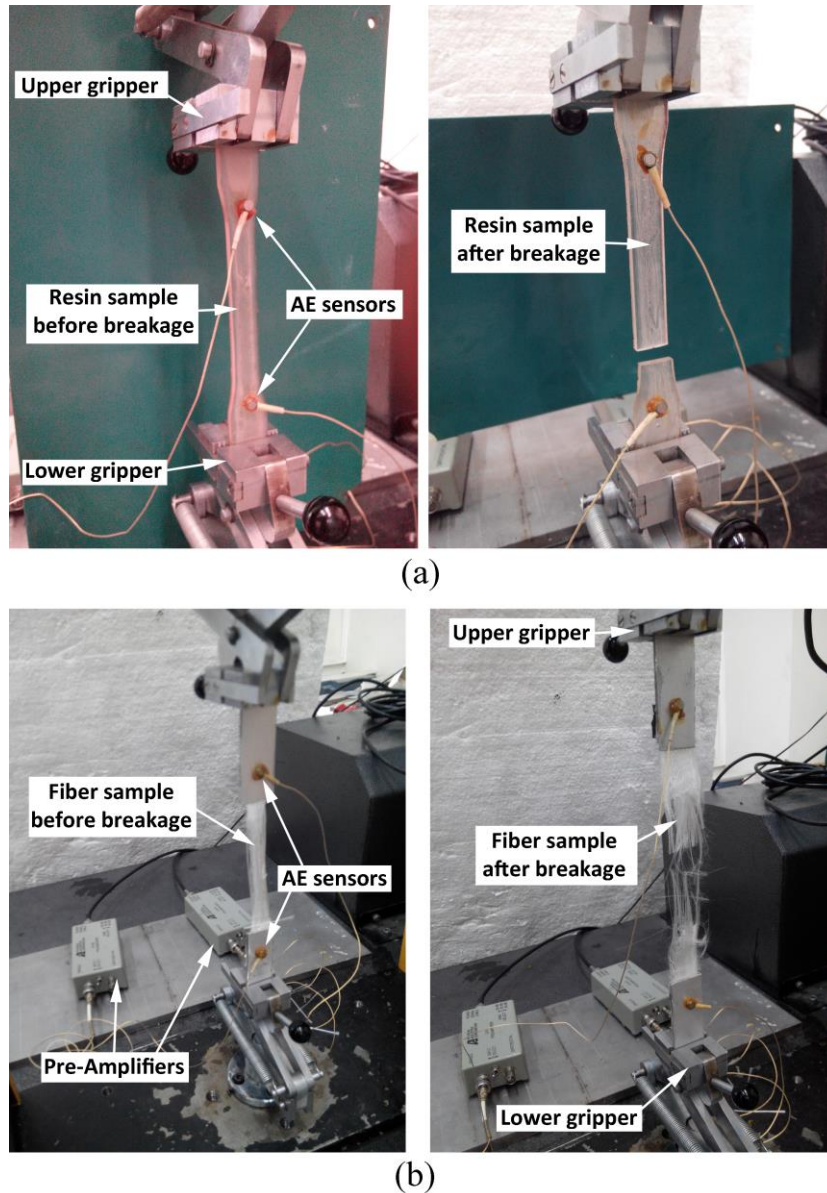


(a)



(b)

Fig. 5 shows frequency distribution of the recoded AE signals during the loading of specimen $U_{S1}$.
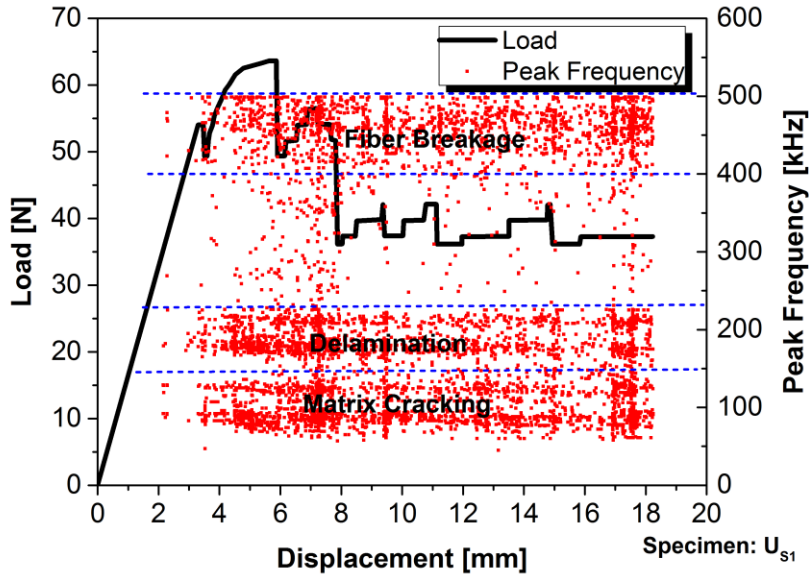
Fig. 5 shows load-displacement and cumulative AE energy-displacement curves for specimens $U_{S1}$ and $W_{S1}$. In load-displacement diagrams, several pop-ins are observable which are related to the sudden crack growths and each pop-in is accompanied by a well-defined acoustic energy jump. By applying the load to the specimen as long as the crack is arrested, the strain energy is stored in the specimen. When the stored strain energy reaches to the critical value, the crack propagates and the stored strain energy is released (see Fig. 6). According to Fig. 6, released strain energy at each pop-in ( $dU\big|_{\Delta}$ ), can be calculated by Eq. 1 [43]:

$$dU\big|_{\Delta} = \frac{1}{2}\Delta \cdot dP \tag{1}$$

where $\Delta$ and dP are displacement and load drop, respectively.

A part of this released energy transmitted within the specimen in the form of stress waves [40], which the AE sensors recorded these waves as AE signals. Thus, the energy

of recorded AE signals ($\Delta E_{AE}$) is some proportion of the available elastic energy ($\Delta U$),

i.e. []:

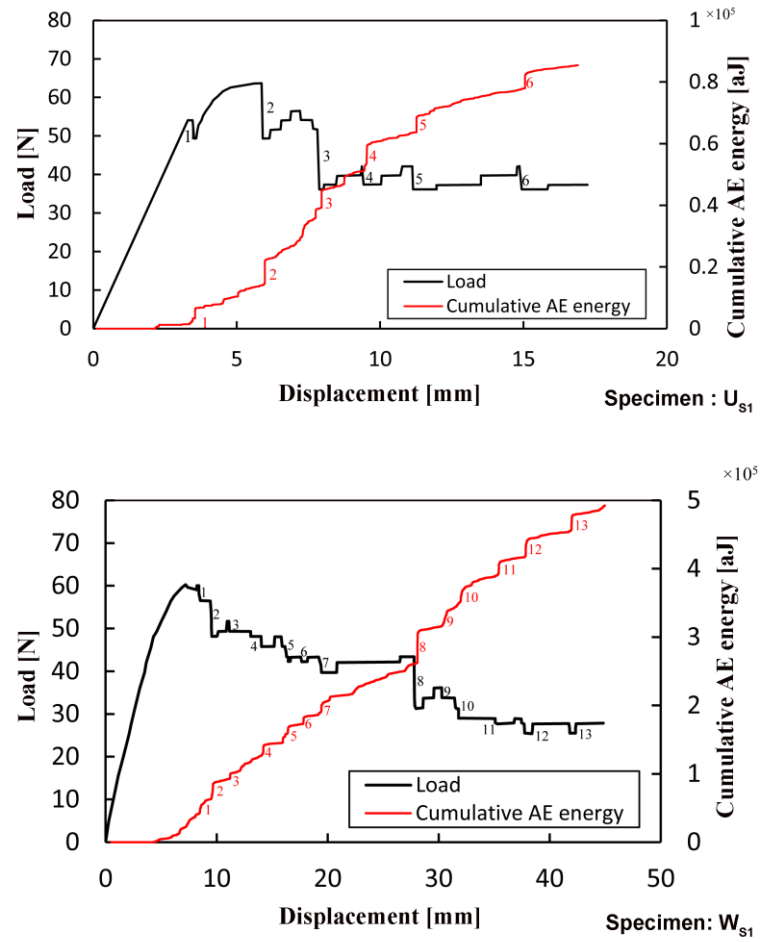$$\Delta U \sim \Delta E_{AE} \hspace{8cm} (2)$$



Fig. 5. Load-displacement and cumulative AE energy curves for specimens $U_{S1}$
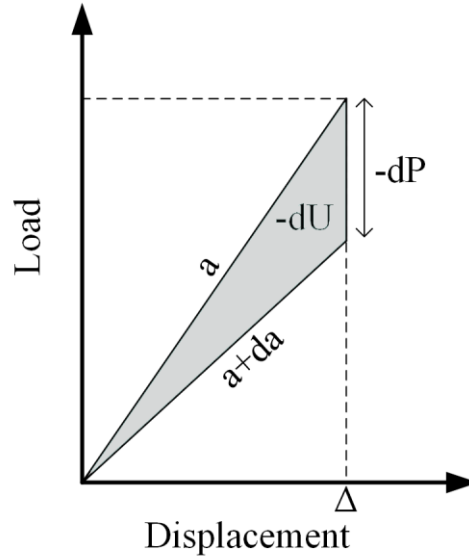
and $W_{S1}$.

**Fig. 6. Changing the strain energy due to infinitesimal crack growth under displacement control mode (a and da are crack length and infinitesimal crack growth, respectively).**

Using Eq. 1, released strain energy at each pop-in was calculated. The corresponding AE energy jump at each pop-in was also calculated using the AE data recorded by the AE sensors. The obtained values of released strain energy (dU) and corresponded AE energy jump ($dE_{AE}$) at each pop-in are represented in Tables 1 and 2.

**Table 1. The values of released strain energy (dU) and AE energy jump ($dE_{AE}$) at each pop-in for specimen $U_{S1}$.**

| Pop-in number | $\Delta$ (mm) | $P_1$ (N) | $P_2$ (N) | dP (N) | $E_{AE\text{-}1}$ ($\times 10^{-14}$ J) | $E_{AE\text{-}2}$ ($\times 10^{-14}$ J) | $dE_{AE}$ ($\times 10^{-14}$ J) | dU ($\times 10^{-3}$ J) |
|---|---|---|---|---|---|---|---|---|
| 1 | 3.46 | 54.03 | 49.32 | 4.71 | 0.34 | 0.66 | 0.32 | 8.15 |
| 2 | 5.87 | 63.67 | 49.33 | 14.34 | 1.45 | 2.22 | 0.77 | 42.09 |
| 3 | 7.63 | 54.09 | 36.13 | 17.96 | 3.36 | 4.48 | 1.12 | 68.52 |
| 4 | 9.37 | 42.08 | 37.37 | 4.71 | 5.16 | 5.63 | 0.47 | 22.07 |
| 5 | 11.10 | 42.12 | 36.14 | 5.98 | 6.37 | 6.86 | 0.49 | 33.19 |
| 6 | 14.80 | 42.13 | 36.15 | 5.98 | 7.79 | 8.28 | 0.49 | 44.25 |

$P_1$: the initial load at each pop-in, $P_2$: the final load at each pop-in, $dP=P_1-P_2$, $E_{AE\text{-}1}$: the initial cumulative AE energy at each pop-in, $E_{AE\text{-}2}$: the final cumulative AE energy at each pop-in, $dE_{AE}=E_{AE\text{-}2}-E_{AE\text{-}1}$.

**Table 2. The values of released strain energy (dU) and AE energy jump (dE$_{AE}$) at each pop-in for specimen W$_{S1}$.**

| Pop-in number | Δ (mm) | P$_1$ (N) | P$_2$ (N) | dP (N) | E$_{AE-1}$ (×10$^{-14}$ J) | E$_{AE-2}$ (×10$^{-14}$ J) | dE$_{AE}$ (×10$^{-14}$ J) | dU (×10$^{-3}$ J) |
|---|---|---|---|---|---|---|---|---|
| 1 | 8.40 | 60.02 | 56.52 | 3.50 | 4.14 | 5.27 | 1.13 | 14.70 |
| 2 | 9.42 | 56.47 | 48.14 | 8.33 | 6.27 | 8.52 | 2.25 | 39.23 |
| 3 | 11.10 | 51.70 | 49.36 | 2.34 | 9.39 | 10.00 | 0.61 | 12.99 |
| 4 | 13.10 | 48.14 | 45.76 | 2.38 | 13.10 | 14.30 | 1.20 | 15.59 |
| 5 | 15.90 | 48.04 | 42.31 | 5.73 | 14.70 | 16.80 | 2.10 | 45.56 |
| 6 | 17.60 | 43.31 | 42.21 | 1.10 | 17.30 | 18.20 | 0.90 | 9.68 |
| 7 | 19.20 | 43.32 | 39.71 | 3.61 | 18.60 | 20.40 | 1.80 | 34.66 |
| 8 | 27.80 | 43.37 | 31.87 | 11.5 | 26.30 | 30.90 | 4.60 | 159.85 |
| 9 | 30.30 | 36.16 | 33.83 | 2.33 | 32.00 | 33.80 | 1.80 | 35.30 |
| 10 | 31.40 | 33.72 | 29.00 | 4.72 | 34.80 | 37.00 | 2.20 | 74.10 |
| 11 | 35.10 | 28.95 | 27.68 | 1.27 | 39.00 | 40.60 | 1.60 | 22.28 |
| 12 | 37.40 | 28.84 | 25.50 | 3.34 | 41.90 | 44.20 | 2.30 | 62.46 |
| 13 | 41.70 | 27.78 | 25.50 | 2.28 | 45.60 | 47.90 | 2.30 | 47.54 |

P$_1$: the initial load at each pop-in, P$_2$: the final load at each pop-in, dP=P$_1$-P$_2$, E$_{AE-1}$: the initial cumulative AE energy at each pop-in, E$_{AE-2}$: the final cumulative AE energy at each pop-in, dE$_{AE}$=E$_{AE-2}$-E$_{AE-1}$.

Fig. 7 illustrates the correlation between AE energy jump and released strain energy at the pop-ins. As can be seen, a linear relationship established between the AE energy jump and released strain energy. Thus, amount of AE energy induced by crack growth, is a function of released strain energy of the specimen.
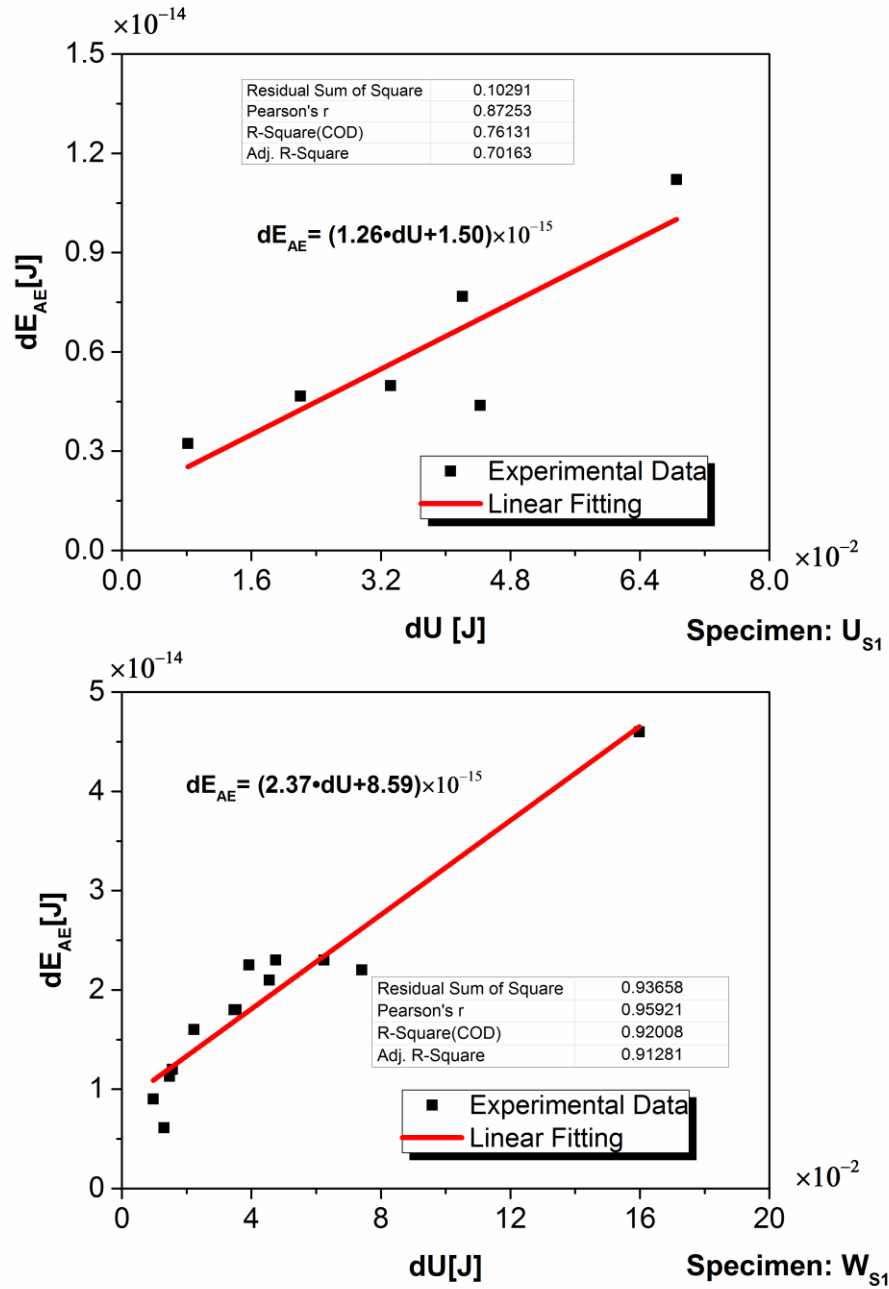
**Fig. 7. Correlation between AE energy jump and strain energy drop at the pop-ins for specimens U$_{S1}$ and W$_{S1}$.**

Strain energy release rate in mode I (G$_I$) for DCB specimen is calculated as follow []:

$$G_I = -\frac{1}{B}\left(\frac{dU}{da}\right)_\Delta = \frac{12P^2a^2}{EB^2h^3} \qquad (3)$$

where B is specimen width, P is load, a is initial crack length, E is young modulus, U is released strain energy, and h is a half thickness of the specimen. Thus, the elastic released strain energy $\Delta U$ due to growth of delamination as much as $\Delta a$ is calculated as follows:

$$dU = -\frac{12P^2a^2}{EBh^3}da \qquad (4)$$

$$\int_0^{\Delta U} dU = -\int_a^{a+\Delta a} \frac{12P^2a^2}{EBh^3}da \qquad (5)$$

$$\Delta U = -\frac{4P^2}{EBh^3}\left[(a+\Delta a)^3 - a^3\right] = \alpha P^2\left[(a+\Delta a)^3 - a^3\right] \qquad (6)$$

Combining Eqs. 2 and 6 leads to

$$\Delta E_{AE} = \beta P^2\left[(a+\Delta a)^3 - a^3\right] \qquad (7)$$

Using $x^3 - y^3 = (x-y)(x^2 + xy + y^2)$ substitution, Eq. 7 modified as follow:

$$\Delta E_{AE} = \beta P^2\left[(a+\Delta a)^3 - a^3\right] = \beta P^2\left[\Delta a^3 + 3a\Delta a^2 + 3a^2\Delta a\right] \qquad (8)$$

Finally, Eq. 8 can be simplified as follow:

$$E_{AE} = \alpha\Delta a^3 + \beta\Delta a^2 + \gamma\Delta a + \eta \qquad (9)$$

Fig. 8 shows the relation between cumulative crack growth and cumulative AE energy for specimens $U_{S1}$ and $W_{S1}$. Due to high value of R-square for the fittings (i.e. 0.97778 and 0.99644 for specimens $U_{S1}$ and $W_{S1}$, respectively.), it is concluded that the 3-order polynomial of Eq. 9 expresses the relation between $E_{AE}$ and $\Delta a$ very well.

The first chart shows "Cumulative AE Energy [aJ]" (×10⁴) versus "Visual Crack Growth [mm]" for Specimen: U$_{S1}$, with Experimental Data and 3-Order Polynomial Fitting.

| Equation | y = Intercept + B1*x^1 + B2*x^2 + B3*x^3 |
|---|---|
| Intercept | 679.73163 |
| B1 | 709.20633 |
| B2 | 17.01622 |
| B3 | -0.30302 |
| Residual Sum of Sq | 9.41729E7 |
| R-Square(COD) | 0.97715 |
| Adj. R-Square | 0.97312 |

Specimen: U$_{S1}$

The second chart shows "Cumulative AE Energy [aJ]" (×10⁵) versus "Visual Crack Growth [mm]" for Specimen: W$_{S1}$, with Experimental Data and 3-Order Polynomial Fitting.

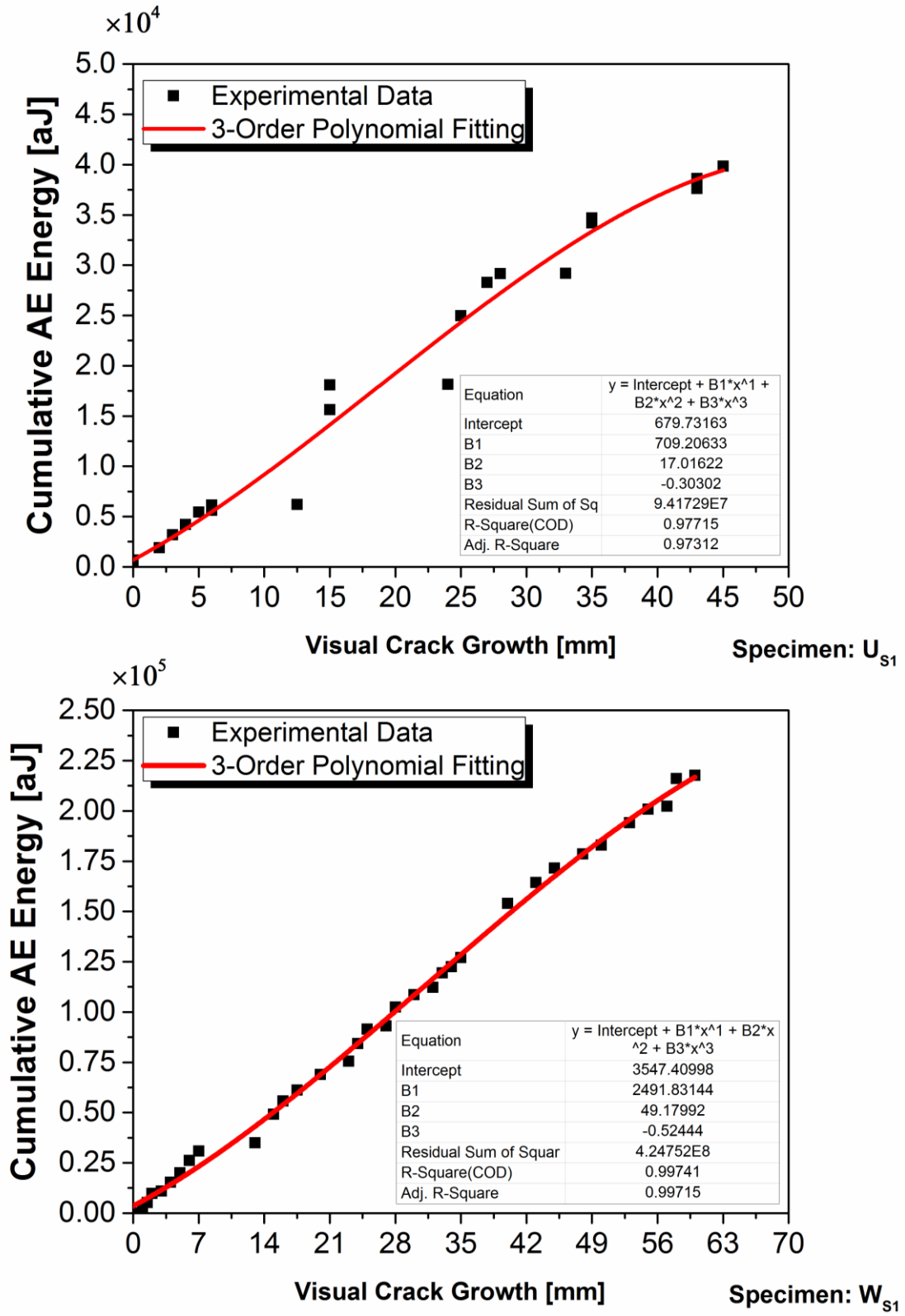| Equation | y = Intercept + B1*x^1 + B2*x^2 + B3*x^3 |
|---|---|
| Intercept | 3547.40998 |
| B1 | 2491.83144 |
| B2 | 49.17992 |
| B3 | -0.52444 |
| Residual Sum of Squar | 4.24752E8 |
| R-Square(COD) | 0.99741 |
| Adj. R-Square | 0.99715 |

Specimen: W$_{S1}$

**Fig. 8. Correlation between visual crack growth and cumulative AE energy for specimens U$_{S1}$ and W$_{S1}$.**

The real root of Eq. 9 at a specific cumulative AE energy determines the value of crack growth. Fig. 9 shows the delamination crack growth estimated by cumulative AE energy versus visually recorded experimental data. As it is obvious, excellent agreement exists between the results. In order to qualify the performance of the proposed method in different loading condition, two other specimens were tested with 1 mm/min loading rate. Fig. 10 shows the predicted delamination propagation curve versus the visually recorded curve for these specimens. As can be seen, by changing the loading condition, AE still can predict delamination propagation precisely.
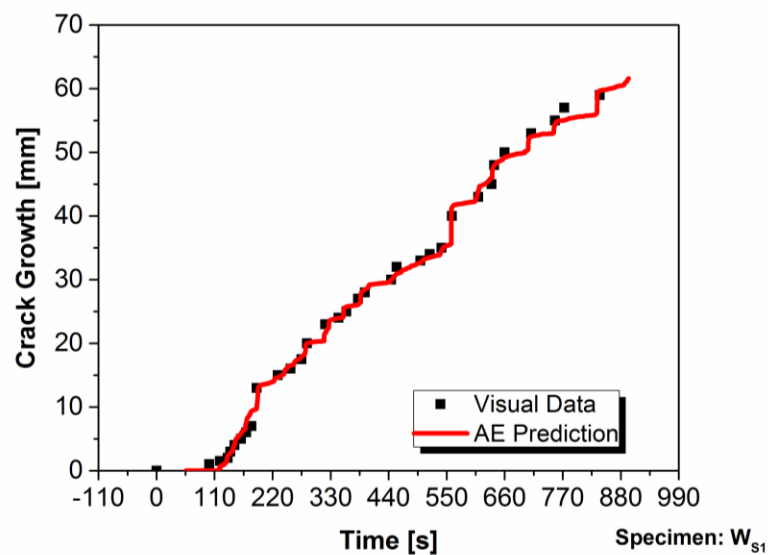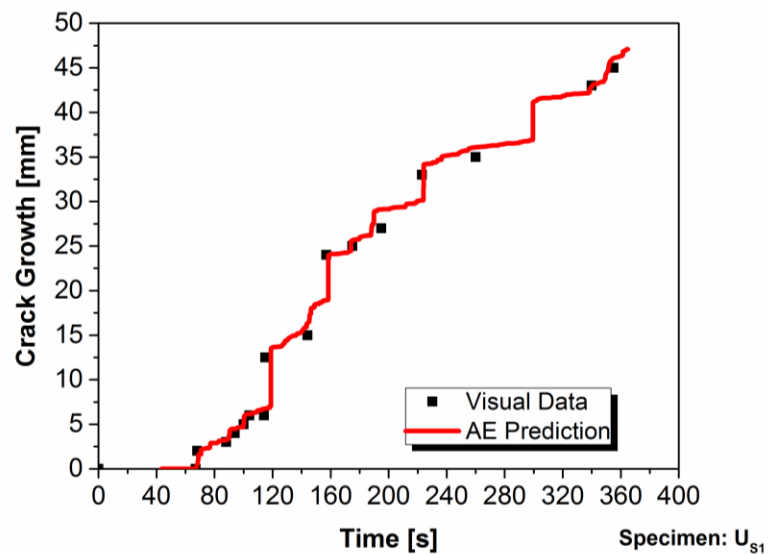
**Fig. 9. Prediction of crack growth using AE method for specimens U$_{S1}$ and W$_{S1}$.**
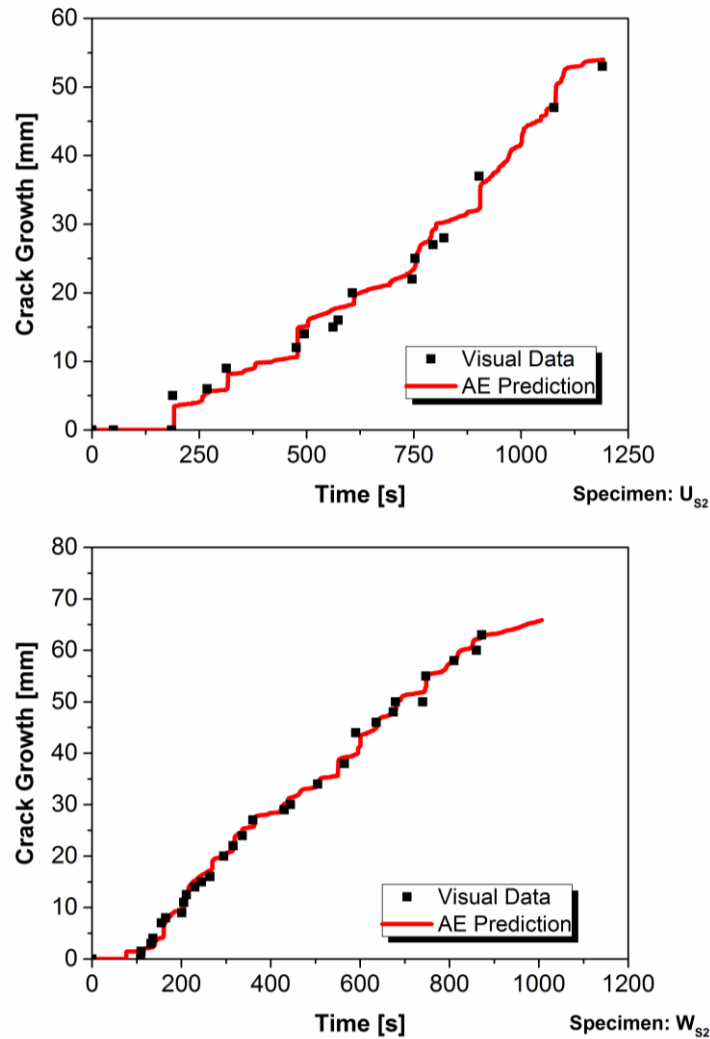


**Fig. 10. Prediction of crack growth using AE method for specimens U$_{S2}$ and W$_{S2}$.**

Table 3 represents the average and maximum differences between the predicted delamination crack growth by AE method and the visually detected crack growth. The results show that the proposed AE method has a good performance to predict quasi-static delamination crack growth.

**Table 3. The maximum and average error of the AE crack growth prediction.**

| Specimens | Loading rate (mm/min) | Maximum error (mm) | Average error (mm) |
|---|---|---|---|
| $U_{S1}$ | 3 | 2.57 | 1.15 |
| $W_{S1}$ | 3 | 1.81 | 0.89 |
| $U_{S2}$ | 1 | 3.01 | 1.16 |
| $W_{S2}$ | 1 | 1.80 | 0.73 |

## *3.2 Fatigue loading*

The samples similar to quasi-static specimens were subjected to the fatigue loading. The tests are performed according to ASTM D6115 standard [39] under displacement control mode. The specifications of the fatigue loading tests are represented in Table 4.

**Table 4. The specifications of the cyclic loading tests.**

| Specimens | Load frequency (Hz) | $\dfrac{\delta_{max}^2}{[\delta_{cr}]_{av}^2} = \dfrac{G_{Imax}}{G_{Ic}}$ | $\delta_{min}$ (mm) | $\delta_{max}$ (mm) | $R = \dfrac{\delta_{min}}{\delta_{max}}$ |
|---|---|---|---|---|---|
| $U_{F1}$ | 3 | 0.8 | 1.2 | 3 | 0.4 |
| $W_{F1}$ | 3 | 0.8 | 2.4 | 6 | 0.4 |
| $U_{F2}$ | 3 | 0.5 | 0.9 | 2.3 | 0.4 |
| $W_{F2}$ | 3 | 0.5 | 2 | 5 | 0.4 |

$\delta_{min}$: minimum displacement for cyclic loading, $\delta_{max}$: maximum displacement for cyclic loading, $\delta_{cr}$: displacement corresponding to crack initiation for quasi-static loading, $G_{Imax}$: fracture energy release rate corresponded to $\delta_{max}$ for cyclic loading, $G_{Ic}$: interlaminar fracture toughness calculated from quasi-static mode I loading.

Fatigue crack growth curves for specimens $U_{F1}$ and $W_{F1}$ are illustrated in Fig. 11. As can be seen, the fatigue crack growth in woven specimen ($W_{F1}$) is more stable than unidirectional specimen ($U_{F1}$). Similar to the quasi-static loading, instability of fatigue crack growth in specimen $U_{F1}$ refers to the fiber bridging phenomenon.
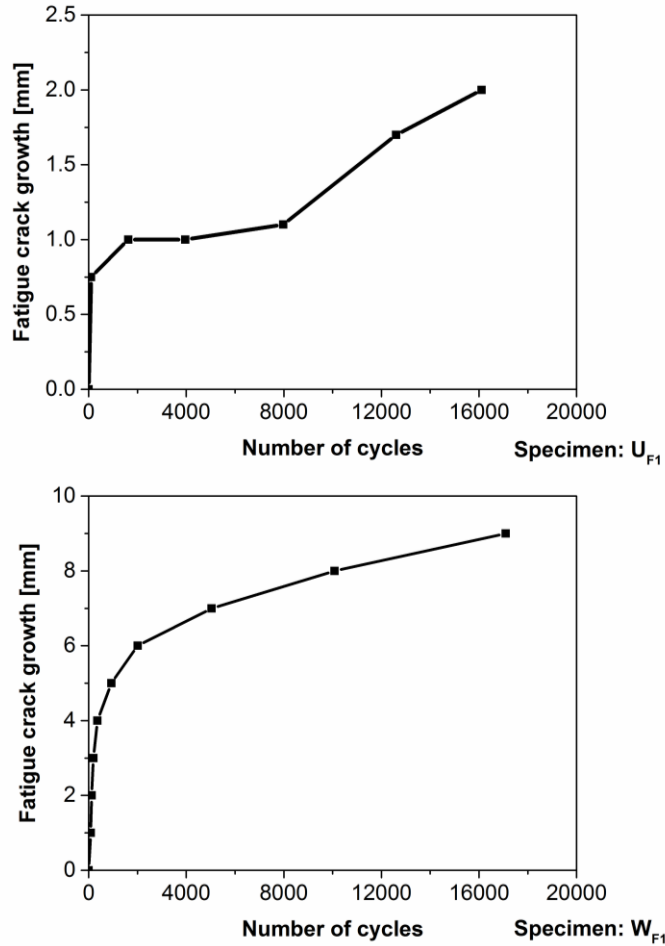
**Fig. 11. The fatigue crack growth for specimens U$_{F1}$ and W$_{F1}$.**

## 3.3 Prediction of fatigue crack growth using AE

Cumulative AE energy of specimens U$_{F1}$ and W$_{F1}$ are illustrated in Fig. 12. By comparing Figs. 11 and 12, it is obvious that the cumulative AE energy curve has similar trend to the fatigue crack growth curve. Thus, similar to the relation between delamination growth and cumulative AE energy in quasi-static loading, there is linear relation between cumulative fatigue crack growth and cumulative AE energy.
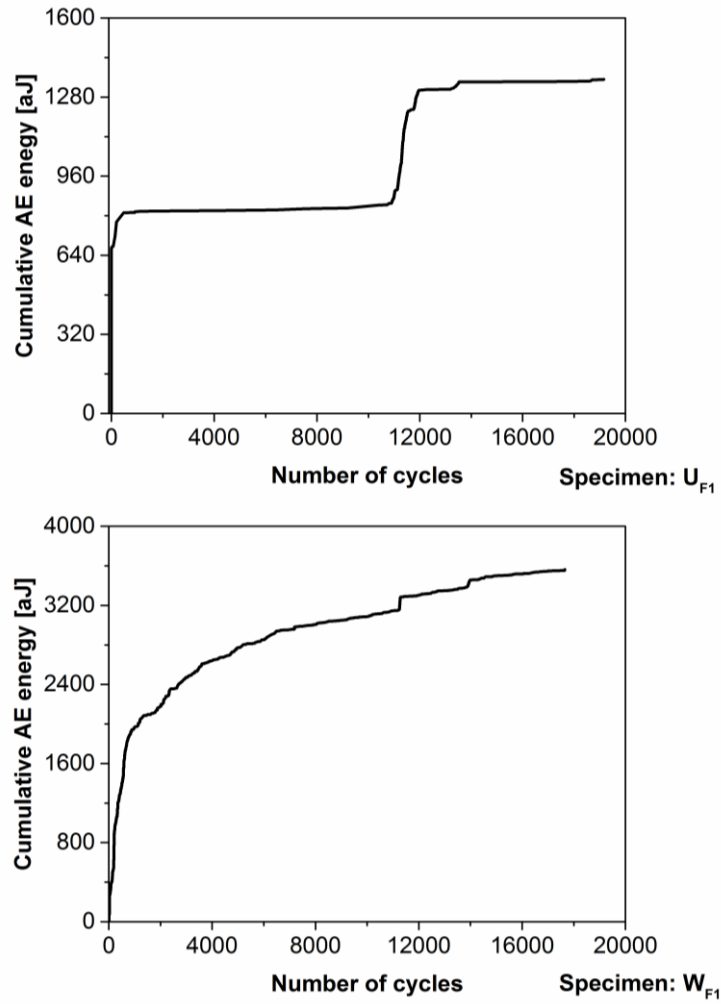
**Fig. 12. Cumulative AE energy curve of specimens U$_{F1}$ and W$_{F1}$.**

Fig. 13 shows the linear relationship between the cumulative fatigue crack growth and cumulative AE energy for specimens U$_{F1}$ and W$_{F1}$.
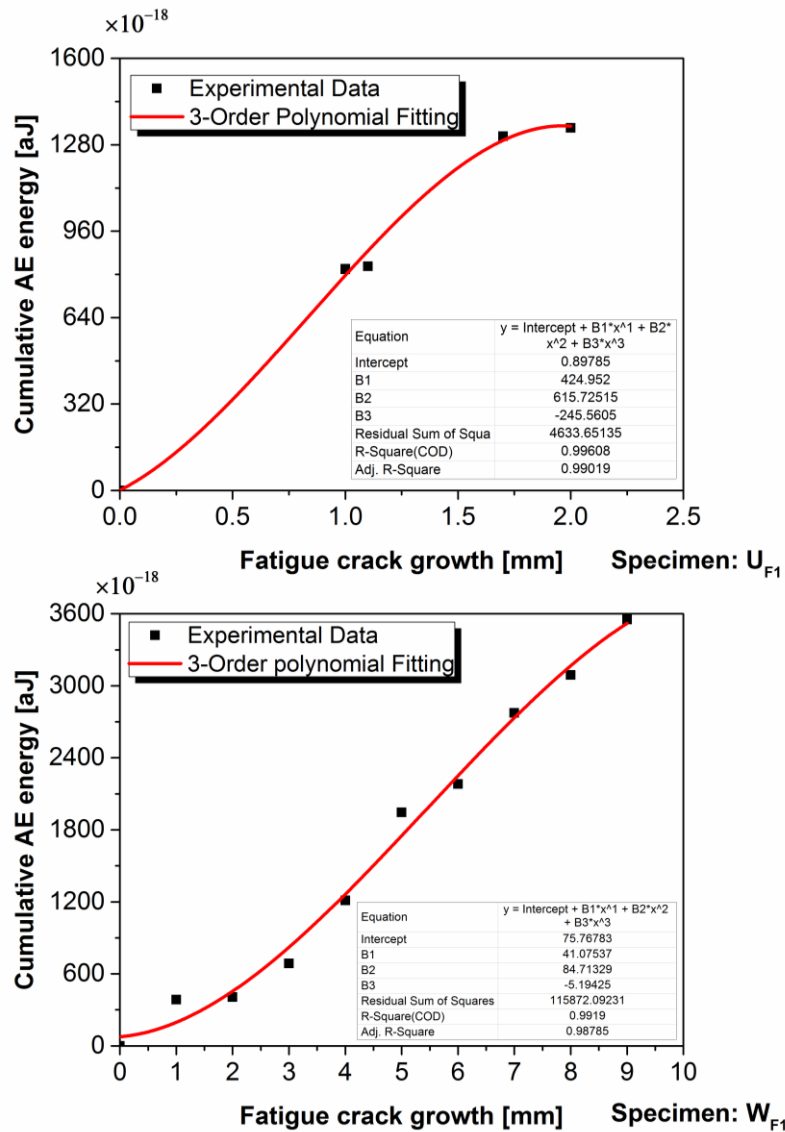
**Fig. 13. Correlation between fatigue crack growth and cumulative AE energy for specimens $U_{F1}$ and $W_{F1}$.**

Fig. 14 illustrates the predicted fatigue crack growth and visually recorded crack growth for specimens $U_{F1}$ and $W_{F1}$. The results show that this method could predict the fatigue crack growth precisely.
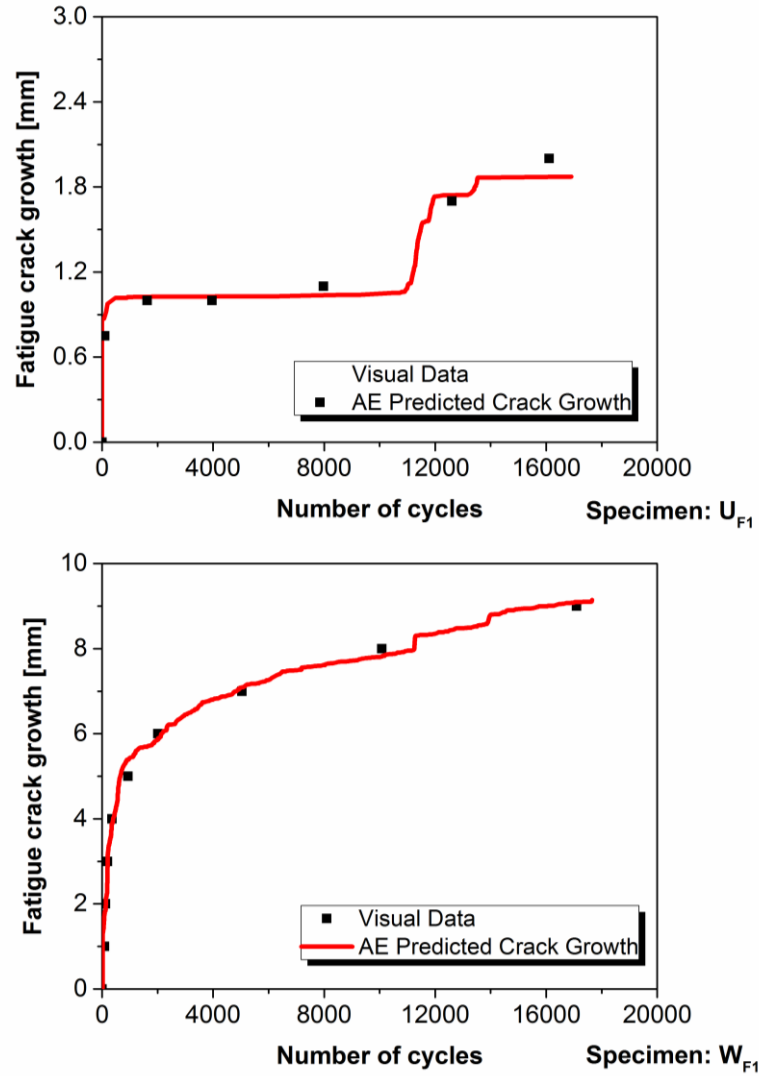
**Fig. 14. Predicted and visually detected delamination fatigue crack growth for specimens U_F1 and W_F1.**

In order to qualify the performance of the proposed method for different fatigue loading conditions, the specimens $U_{F2}$ and $W_{F2}$ were tested under lower stress levels

($\dfrac{\delta_{max}^2}{[\delta_{cr}]_{av}^2} = \dfrac{G_{Im\,ax}}{G_{Ic}} = 0.5$). The predicted fatigue crack growth curve for these specimens
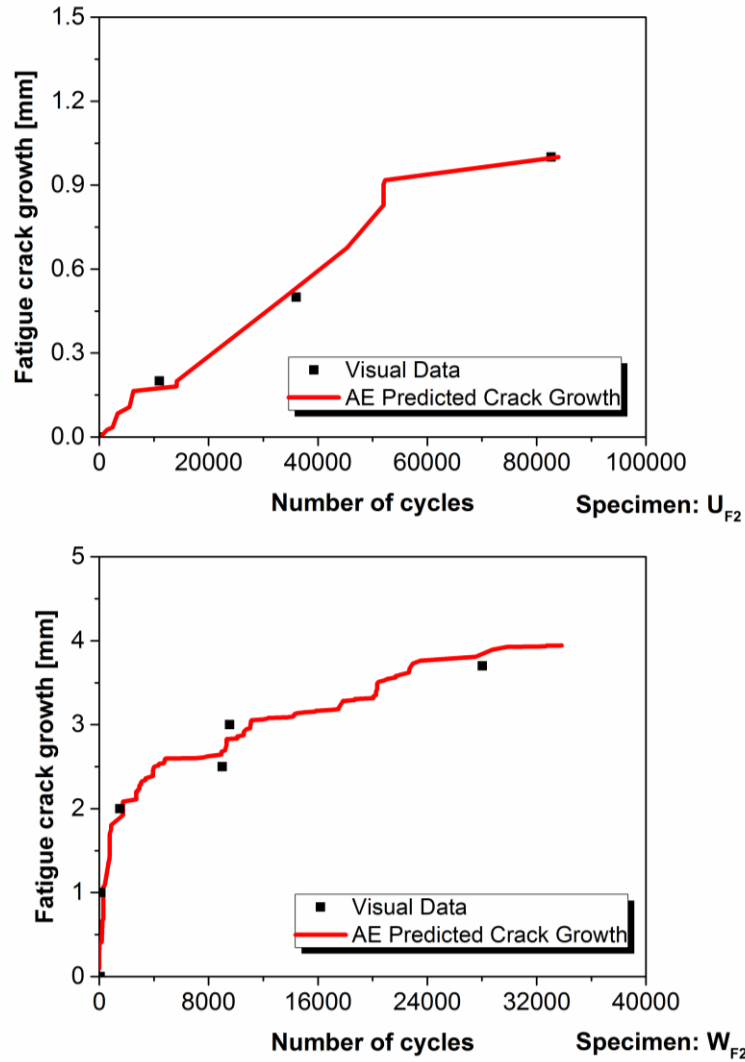
are illustrated in Fig. 15.

**Fig. 15. Predicted and visually detected delamination fatigue crack growth for specimens U_F2 and W_F2.**

Table 5 represents the average and maximum differences between the predicted fatigue crack growth by AE method and the visually detected fatigue crack growth. The results show that the proposed AE method has an excellent performance to predict fatigue delamination crack growth.

**Table 5. The maximum and average error of the AE fatigue crack growth prediction.**

| Specimens | $\dfrac{G_{Imax}}{G_{Ic}}$ | Maximum error (mm) | Average error (mm) |
| --- | --- | --- | --- |
|  |  |  |  |

| | | | |
|---|---|---|---|
| $U_{F1}$ | 0.8 | 0.14 | 0.07 |
| $W_{F1}$ | 0.8 | 0.31 | 0.15 |
| $U_{F2}$ | 0.5 | 0.12 | 0.08 |
| $W_{F2}$ | 0.5 | 0.20 | 0.14 |

# 4 Conclusion

The aim of this study was to investigate the delamination propagation in glass/epoxy composites under mode I quasi-static and fatigue loading conditions. The results are represented in two sections. In first section, correlations among AE energy with released strain energy and crack growth are established and quasi-static delamination growth was predicted using AE method. In second section, the delamination crack growth under fatigue loading is predicted using the proposed AE method. The proposed AE method has some advantages such as predicting delamination growth using only one AE sensor without needing to determine AE wave propagation velocity in the specimens and without need to filtering some AE recorded signals. Finally, the obtained results show that the proposed AE method has good applicability to predict the delamination propagation in laminated composite structures.

# References

[1] Batra, R.C., Gopinath, G., Zheng, J.Q.: Damage and failure in low energy impact of fiber-reinforced polymeric composite laminates, Compos. Struct. **94**, 540–7 (2012).

[2] Minak, G., Morelli P., Zucchelli, A.: Fatigue residual strength of circular laminate graphite– epoxy composite plates damaged by transverse load. Compos. Sci. Technol. **69**, 1358–63 (2009).

[3] Ramadas, C., Balasubramaniam, K., Joshi, M., Krishnamurthy, C.V.: Characterisation of rectangular type delaminations in composite laminates through B- and D-scan images generated using Lamb waves. NDT&E Int. **44**(3), 281-9 (2011).

[4] Rolfes, R., Ernst, G., Vogler, M., Hühne, C.: Material and failure models for textile composites. In: Camanho, P.P., Dávila, C.G., Pinho, S.T., Remmers, J.J.C., editors.: Mechanical response of composites. Springer, 27-56 (2008)

[5] Mechraoui, S.E., Laksimi, A., Benmedakhene, S.: Reliability of damage mechanism localization by acoustic emission on glass/epoxy composite material plate. Compos. Struct. **94**, 1483–94 (2012)

[6] Ativitavas, N., Fowler, T.J., Pothisiri, T.: Identification of fiber breakage in fiber reinforced plastic by low-amplitude filtering of acoustic emission data. J. Nondestr. Eval. 23(1), 21-36 (2004)

[7] Arumugam, V., Suresh Kumar, C., Santulli, C., Sarasini, F., Stanley, A.J.: A global method for the identification of failure modes in fiberglass using acoustic emission. J. Test. Eval. **39**(5), 1-13 (2011)

[8] Sasikumar, T., Rajendraboopathy, S., Usha, K.M., Vasudev, E.S.: Artificial neural network prediction of ultimate strength of unidirectional T-300/914 tensile specimens using acoustic emission response. J. Nondestr. Eval. 27(4), 127–133 (2008)

[9] Sridharan, S.: Delamination behaviour of composites. CRC Press, New York, (2008)

[10] Liu, P., Groves, R.M., Benedictus, R.: 3D monitoring of delamination growth in a wind turbine blade composite using optical coherence tomography. NDT&E Int. **64**, 52-8 (2014)

[11] Allegri, G., Wisnom, M.R., Hallett, S.R.: A new semi-empirical law for variable stress-ratio and mixed-mode fatigue delamination growth. Composites Part A. **48**, 192–200 (2013)

[12] Chen, J.F., Morozov, E.V., Shankar, K.: Simulating progressive failure of composite laminates including in-ply and delamination damage effects. Composites Part A. **61**, 185–200 (2014)

[13] Canturri, C., Greenhalgh, E.S., Pinho, S.T., Ankersen, J.: Delamination growth directionality and the subsequent migration processes – The key to damage tolerant design. Composites Part A. **54**, 79–87 (2013)

[14] Hosseini Toudeshky, H., Hosseini, S., Mohammadi, B.: Delamination buckling growth in laminated composites using layerwise-interface element. Compos. Struct. **92**, 1846–56 (2010)

[15] Benzeggagh, M.L., Kenane, M.: Measurement of mixed-mode delamination fracture toughness of unidirectional glass/epoxy composites with mixed-mode bending apparatus. Compos. Sci. Technol. **56**, 439-49 (1996)

[16] Fotouhi, M., Ahmadi Najafabadi, M.: Investigation of the mixed-mode delamination in polymer-matrix composites using acoustic emission technique. J. Reinf. Plast. Compos. **33**(19), 1767-82 (2014)

[17] Camanho, P.P., Davila, C.G., De Moura, M.F.: Numerical simulation of mixed-mode progressive delamination in composite materials. J. Compos. Mater. **37** (16), 1415-38 (2003)

[18] Aghazadeh Mohandesi, J., Majidi, B.: Fatigue damage accumulation in carbon/epoxy laminated composites. Mater. Des. **30**, 1950–6 (2009)

[19] Chen, D., Gilbert, C.J., Ritchie, O.: In situ measurement of fatigue crack growth rates in a silicon carbide ceramic at elevated temperatures using a DC potential system. J. Test. Eval. **28**(4), 236-41 (2000)

[20] Miller, R.K.: Nondestructive testing Handbook: Acoustic emission testing. 5 ed, American Society for Nondestructive Testing, (1987)

[21] Kostopoulos, V., Loutas, T., Dassios, K.: Fracture behavior and damage mechanisms identification of SiC/glass ceramic composites using AE monitoring. Compos. Sci. Technol. **67**, 1740–6 (2007)

[22] Zhuang, X., Yan, X.: Investigation of damage mechanisms in self-reinforced polyethylene composites by acoustic emission. Compos. Sci. Technol. **66** (3–4), 444–9 (2006)

[23] McCrory, J.P., Al-Jumaili, S.K., Crivelli, D., Pearson, M.R., Eaton, M.J., Featherston, C.A., Guagliano, M., Holford, K.M., Pullin, R.: Damage classification in carbon fibre composites using acoustic emission: A comparison of three techniques. Composites Part B. **68**, 424–30 (2015)

[24] Fotouhi, M., Heidary, H, Ahmadi, M., Pashmforoush, F.: Characterization of composite materials damage under quasi-static three point bending test using wavelet and fuzzy c-means clustering, J. Compos. Mater. **46**(15), 1795–808 (2012)

[25] Mizutani, Y., Nagashima, K., Takemoto, M., Ono, K.: Fracture mechanism characterization of cross-ply carbon-fiber composites using acoustic emission analysis. NDT&E Int. **33**(2), 101-10 (2000)

[26] Pashmforoush, F., Khamedi, R., Fotouhi, M., Hajikhani, M., Ahmadi, M.: Damage classification of sandwich composites using acoustic emission technique and k-means genetic algorithm. J. Nondestr. Eval. **33**(4), 481–492 (2014)

[27] Suresh Kumar, C., Arumugam, V., Sajith, S., Dhakal, H.N., John, R.: Acoustic emission characterisation of failure modes in hemp/epoxy and glass/epoxy composite laminates. J. Nondestruct. Eval. 34: 31 (2015)

[28] Refahi Oskouei, A., Ahmadi, M.: Acoustic emission characteristics of mode I delamination in glass/polyester composites. J. Compos. Mater. **44**(7), 793-807 (2010)

[29] Martínez-Jequier, J., Gallego, A., Suárez, E., Juanes, F.J., Valea, Á.: Real-time damage mechanisms assessment in CFRP samples via acoustic emission Lamb wave modal analysis. Composites Part B. **68**, 317–26 (2015)

[30] Fotouhi, M., Saeedifar, M., Sadeghi, S., Ahmadi Najafabadi, M., Minak, G.: Investigation of the damage mechanisms for mode I delamination growth in foam core sandwich composites using acoustic emission. Struct. Health. Monit. **14**(3), 265-80. (2015)

[31] Taghizadeh, J., Ahmadi, M.: Identification of damage modes in polypropylene/epoxy composites by using principal component analysis on AE signals extracted from Mode I delamination, Nondestruct. Test. Eval. **27**(2), 151-70 (2012)

[32] Silversides, I., Maslouhi, A., Laplante, G.: Interlaminar fracture characterization in composite materials by using acoustic emission. 5th International Symposium on NDT in Aerospace, Singapore, (2013)

[33] Fotouhi, M., Ahmadi Najafabadi, M.: Acoustic emission-based study to characterize the initiation of delamination in composite materials. J. Thermoplast. Compos. Mater. **29**(4), 519-37 (2016)

[34] Arumugam, V., Sajith, S., Stanley, A.J.: Acoustic emission characterization of failure modes in GFRP laminates under mode I delamination, J. Nondestr. Eval. **30**(3), 213-9 (2011)

[35] Saeedifar, M., Fotouhi, M., Ahmadi Najafabadi, M., Hosseini Toudeshky, H.: Interlaminar fracture toughness evaluation in glass/epoxy composites using acoustic emission and finite element methods. J. Mater. Eng. Perform. **24**(1), 373-84 (2015)

[36] Silversides, I., Maslouhi, A., Laplante, G.: Acoustic emission monitoring of interlaminar delamination onset in carbon fibre composites. Struct. Health. Monit. **12**(2), 126-40 (2013)

[37] Romhany, G., Szebényi, G.: Interlaminar fatigue crack growth behavior of MWCNT/carbon fiber reinforced hybrid composites monitored via newly developed acoustic emission method. Express. Polym. Lett. **6**(7), 572-80 (2012)

[38] ASTM D5528-01. Standard test method for mode I interlaminar fracture toughness of unidirectional fiber-reinforced polymer matrix composites. ASTM International, West Conshohocken, PA., (2007)

[39] ASTM D6115−97: Standard test method for mode I fatigue delamination growth onset of unidirectional fiber-reinforced polymer matrix composites. ASTM International, West Conshohocken, PA., (2011)

[40] Mandorini, V., Ghelardoni, E., Tribuno, C.: Acoustic energy during pop-in crack propagation, Eng. Fract. Mech. **15**(3-4), 255-73 (1981)

[41] Hiley, M.J.: Delamination between multi-directional ply interfaces in carbon-epoxy composites under static and fatigue loading. In: Williams, J.G., Pavan, A., editors.: Fracture of polymers, composites, and adhesives. Elsevier, 61-72 (2000)

[42] Andersons, J., König, M.: Dependence of fracture toughness of composite laminates on interface ply orientations and delamination growth direction. Compos. Sci. Technol. **64**(13–14), 2139–52 (2004)

[43] Anderson, T.L.: Fracture Mechanics; fundamentals and applications. 4th ed. Taylor & Francis, (2005)

# List of Figure captions

**Fig. 1.** The specimens geometry and dimensions.

**Fig. 2.** The experimental setup for quasi-static and fatigue tests.

**Fig. 3.** Load-displacement and crack growth-displacement diagrams for specimens $U_{S1}$ and $W_{S1}$.

**Fig. 4.** Fiber bridging and crack plane changing in specimen a) $U_{S1}$, and b) $W_{S1}$.

**Fig. 5.** Load-displacement and cumulative AE energy curves for specimens $U_{S1}$ and $W_{S1}$.

**Fig. 6.** Changing the strain energy due to infinitesimal crack growth under displacement control mode.

**Fig. 7.** Correlation between AE energy jump and strain energy drop at the pop-ins for specimens $U_{S1}$ and $W_{S1}$.

**Fig. 8.** Correlation between visual crack growth and cumulative AE energy for specimens $U_{S1}$ and $W_{S1}$.

**Fig. 9.** Prediction of crack growth using AE method for specimens $U_{S1}$ and $W_{S1}$.

**Fig. 10.** Prediction of crack growth using AE method for specimens $U_{S2}$ and $W_{S2}$.

**Fig. 11.** The fatigue crack growth for specimens $U_{F1}$ and $W_{F1}$.

**Fig. 12.** Cumulative AE energy curve of specimens $U_{F1}$ and $W_{F1}$.

**Fig. 13.** Correlation between fatigue crack growth and cumulative AE energy for specimens $U_{F1}$ and $W_{F1}$.

**Fig. 14.** Predicted and visually detected delamination fatigue crack growth for specimens $U_{F1}$ and $W_{F1}$.

**Fig. 15.** Predicted and visually detected delamination fatigue crack growth for specimens $U_{F2}$ and $W_{F2}$.

# List of Table captions

**Table 1.** The values of released strain energy (dU) and AE energy jump (dEAE) at each pop-in for specimen $U_{S1}$.

**Table 2.** The values of released strain energy (dU) and AE energy jump (dEAE) at each pop-in for specimen $W_{S1}$.

**Table 3.** The maximum and average error of the AE crack growth prediction.

**Table 4.** The specifications of the cyclic loading tests.

**Table 5.** The maximum and average error of the AE fatigue crack growth prediction.

$$G = -\frac{1}{B}\left(\frac{dU}{da}\right)_{\Delta} = \frac{12P^2a^2}{EB^2h^3}$$

$$dU = -\frac{12P^2a^2}{EBh^3}da$$

$$\int_{0}^{\Delta U} dU = -\int_{a}^{a+\Delta a} \frac{12P^2a^2}{EBh^3}da$$

$$\Delta U = -\frac{4P^2}{EBh^3}\left[(a+\Delta a)^3 - a^3\right] = \alpha P^2\left[(a+\Delta a)^3 - a^3\right]$$

$$\Delta U \sim \Delta E_{AE}$$

$$\Delta E_{AE} = \beta P^2\left[(a+\Delta a)^3 - a^3\right]$$

$$x^3 - y^3 = (x-y)(x^2 + xy + y^2)$$

$$\Delta E_{AE} = \beta P^2\left[(a+\Delta a)^3 - a^3\right] = \beta P^2\left[\Delta a^3 + 3a\Delta a^2 + 3a^2\Delta a\right]$$

$$E_{AE} = \alpha\Delta a^3 + \beta\Delta a^2 + \gamma\Delta a + \eta$$